frontiers | Frontiers in Marine Science

TYPE Original Research
PUBLISHED 23 February 2024
DOI 10.3389/fmars.2024.1284813

OPEN ACCESS

EDITED BY
Andri Frediansyah,
Indonesian Institute of Sciences, Indonesia

REVIEWED BY
Ramasamy Ramasubburayan,
Manonmaniam Sundaranar University, India
Arabinda Ghosh,
Mahapurasha Srimanta Sankaradeva Viswavidyalaya, India
Suriana Sabri,
Putra Malaysia University, Malaysia

*CORRESPONDENCE
Muddukrishnaiah Kotakonda
krishna123muddu@gmail.com

RECEIVED 29 August 2023
ACCEPTED 30 January 2024
PUBLISHED 23 February 2024

CITATION
Pemmadi RV, Alhakamy NA, Asfour HZ, Kotta S, Alfaleh MA, Sunnapu P, Uk I, Pottail L, Chithambharan A, Yogananthan D, Thavamani B S, Valiyaparambil S, Kallungal SM and Kotakonda M (2024) Enhancing antibacterial efficacy and accelerating infectious wound healing in rats using biogenic metal nanoparticles from marine *Bacillus subtilis*. *Front. Mar. Sci.* 11:1284813. doi: 10.3389/fmars.2024.1284813

Enhancing antibacterial efficacy and accelerating infectious wound healing in rats using biogenic metal nanoparticles from marine *Bacillus subtilis*

Raghuveer Varma Pemmadi[1], Nabil Abdulhafiz Alhakamy[2,3], Hani Z. Asfour[2,3], Sabna Kotta[2,3], Mohamed A. Alfaleh[2,3], Prasad Sunnapu[4], Ilyas Uk[5], Lalitha Pottail[6], Akhila Chithambharan[6], Dhanapal Yogananthan[7], Samuel Thavamani B[8], Shilpa Valiyaparambil[9], Sirajudheen Mukriyan Kallungal[9] and Muddukrishnaiah Kotakonda[9]*

[1]Department of Medicinal Chemistry, A.K.R.G. College of Pharmacy, Nallajerla, Andhra Pradesh, India, [2]Department of Pharmaceutics, Faculty of Pharmacy, King Abdulaziz University, Jeddah, Saudi Arabia, [3]Center of Excellence for Drug Research and Pharmaceutical Industries, King Abdulaziz University, Jeddah, Saudi Arabia, [4]Department of Pharmaceutical Chemistry, Sri Ramakrishna Institute of Paramedical Science, College of Pharmacy, Coimbatore, India, [5]Department of Pharmacognosy and Phytochemistry, Moulana College of Pharmacy, Perinthalmanna, Kerala, India, [6]Department of Chemistry and Coordinator, Bharat Ratna, Prof. C. N. R Rao Research Centre, Avinashilingam Institute for Home Science and Higher Education for Women, Coimbatore, India, [7]Department of Pharmacology, PSG Institute of Medical Sciences & Research, Coimbatore, India, [8]Department of Pharmacognosy, Ahalia School of Pharmacy, Kozhipara, Kerala, India, [9]Department of Pharmaceutics, Jamia Salafiya Pharmacy College, Pulikkal, Kerala, India

Introduction: Microorganisms originating from the marine environment, such as bacteria, fungi, and algae, are deliberately employed in the production of nanoparticles on account of the wide array of bioactive compounds they produce.

Methods: Cell-free aqueous extracts of marine *Bacillus subtilis* (CBPPR1) were used to synthesise AuNPs (CBPPR1AuNPs) and AgNPs (CBPPR1AgNPs). Zetasizer Nano ZS (Malvern Instruments) zeta size and zeta potential, field emission and transmission scanning electron microscopy (FE-SEM and HR-TEM), UV-visible (UV-Vis), X-ray diffraction (XRD), Fourier transform infrared (FT-IR), and EDAX were used to characterize biogenically synthesized nanoparticles (NPs). Their antibacterial activities against *Escherichia coli*, *Klebsiella pneumoniae*, and *Staphylococcus aureus* were investigated. The anticancer efficacy of CBPPR1Au and AgNPs was investigated in human colorectal adenocarcinoma cell lines (HT-29, HT-116). CBPPR1AgNPs formulation was studied *in vitro* and *in-vivo* rat models. The assessment focused on its efficacy in wound healing and antibacterial capabilities, comparing them against a commercial product. To determine the effectiveness of CBPPR1AgNPs in wound healing, a cutaneous wound model was employed, which included infection with *S. aureus*.

Results and discusion: CBPPR1Au and AgNPs significantly inhibited the growth of S aureus at MIC of 125 µg (CBPPR1AuNPs) and 62.5 µg (CBPPR1AgNPs) respectively. FE-SEM and HR-TEM observations confirmed that NPs caused bacterial cell leakage, damage, and shrinkage. Cancer cell viability was reduced upon treatment with increasing concentrations of CBPPR1Au and AgNPs, and apoptosis was increased in cells treated with CBPPR1Au and AgNPs relative to untreated cells ($p < 0.001$). CBPPR1Au and AgNPs showed significant cytotoxic activity against HT-29 (15.5 M) and HT-116 (62.5 M) cells. *In-vivo* experiments on rats showed minimal pus formation in groups CBPPR1AgNPs (62.5 µg/ml) G2, CBPPR1AgNPs (125 µg/ml) G3, and silver sulfadiazine G4, indicating the effective control of infections. CBPPR1AgNPs-treated wounds showed complete closure, whereas untreated G1 wounds remained unhealed. Histopathological analysis showed no adverse effects of CBPPR1AgNPs on kidneys and livers of rats. These findings suggest that CBPPR1AgNPs play a pivotal role in wound healing because of their potent antibacterial properties.

KEYWORDS

marine *Bacillus subtilis*, cell-free extraction, gold nanoparticles, silver nanoparticles, antibacterial activity, anticancer activity, *in-vivo* wound healing activity

Introduction

Green materials have become a trend in recent years, and the ethics of protecting the environment is practiced in synthesising materials, leading to the production of green-synthesised nanoparticles. Several different metal nanoparticles have been used in a wide range of medicinal applications. Gold nanoparticles (AuNPs) are recognised as crucial tools in drug delivery systems and have remarkable significance. Owing to their exceptional physicochemical properties, AuNPs have extensive utility across a variety of interdisciplinary fields including medicine, pharmaceutical science, biology, chemistry, and physics (Khan et al., 2019). A wide range of therapeutic uses of AuNPs have been reported, including the transport of drugs and genes, photodynamic and radiation therapy, computed tomography, photothermal therapy, and diagnostic imaging (Hu et al., 2020).

Silver nanoparticles (AgNPs) are highly significant among metallic nanomaterials because of their diverse range of use as antimicrobial agents (Kambale et al., 2020; Singh et al., 2017), catalysts (Fatimah, 2016), tools for chemical and biomolecular detection (Dubas and Pimpan, 2008; Loiseau et al., 2019), and enhancers of Raman scattering (Fang et al., 2015). The distinctive nanoscale reactivity of AgNPs depends on factors such as their size, shape, surface coating, and nanostructured surface chemistry. Therefore, there is much interest in developing synthetic methods that allow AgNPs to regulate their dimensions, shape, distribution, and monodispersity (Zhang et al., 2016; Lee and Jun, 2019).

Microorganisms such as bacteria, fungi, yeast, and algae are commonly employed for nanoparticle synthesis because of their ease of cultivation, rapid growth, and ability to thrive under ambient conditions of pH, temperature, and pressure (Fariq et al., 2017; Ghosh et al., 2021). Various components within microbial cells, including the cell wall, cell membrane, proteins, enzymes, and other intracellular constituents play crucial roles in nanoparticle formation. Parameters such as temperature, pH, biomass, and other physical factors also influence the production of metallic nanoparticles like AgNPs. These nanoparticles offer several health-related benefits including antibacterial, antifungal, and antiviral capabilities (Wei et al., 2009).

Biologically synthesised gold and silver nanoparticles have emerged as promising candidates for anticancer and antimicrobial activities (Ramachandran et al., 2017). The unique properties of these nanoparticles, coupled with the environmentally friendly and sustainable nature of their synthesis, contribute to their therapeutic potential. In the case of cancer, gold nanoparticles, for instance, exhibit remarkable biocompatibility and can be engineered to selectively target cancer cells and precisely deliver therapeutic agents (Soliman et al., 2023; Bharadwaj et al., 2021). Additionally, their plasmonic properties enable them to absorb and convert light into heat, facilitating localised hyperthermia to destroy cancer cells (Vines et al., 2019). On the antimicrobial front, both gold and silver

Abbreviations: NPs, Nanoparticles; CBPPR1, Marine *B. subtilis*; CBPPR1Au, Marine *B. subtilis* extract gold nanoparticles; CBPPR1Ag, Marine *B. subtilis* extract silver nanoparticles; HT-29, Human colorectal adenocarcinoma cell; HT-116, Human colorectal adenocarcinoma cell; AgNPs, Silver nanoparticles; AuNPs, Gold nanoparticles; MIC, Minimum Inhibitory concentration; FESEM, Field emission scanning electronic microscope; HRTEM, High Resolution transmission electronic microscope; MHA, Mueller hinton agar; DMEM, Dulbecco's Modified Eagle's Medium; FACS, fluorescence-activated cell sorting.

nanoparticles possess inherent antimicrobial properties, disrupting microbial membranes and interfering with cellular functions (Mihai et al., 2019). Their diminutive size allows them to penetrate into microbial cells efficiently, enhancing their efficacy against a broad spectrum of pathogens. Furthermore, these nanoparticles can be tailored for specific applications, such as wound dressings or coatings on medical devices, providing an extra layer of protection against infections. The combination of nanotechnology with biology in the synthesis of these nanoparticles shows a harmonious integration of scientific disciplines, holding great promise for the development of advanced and effective therapies against cancer (Jin et al., 2020) and infectious diseases.

This environmentally friendly and cost-effective green synthesis method has established its stability and suitability for large-scale production. These favourable attributes of AuNPs and AgNPs prompted the researchers to choose CBPPR1 as the subject of our study. Green synthesis techniques were utilised to create gold and silver nanoparticles with the assistance of CBPPR1.

Methodology

Isolation of marine *B. subtilis*

Manual sampling was used to collect marine sediment from the Gulf of Mannar (Rameswaram, India). Samples were placed in plastic containers before being sent to the laboratory. Sediment samples were serially diluted in sterile water. Using the spread plate technique, 1mL of each dilution was distributed on Zobell marine agar plates (Himedia, India), which were then incubated at room temperature for two days. The colonies were separated and purified using the streak plate method and CBPPR1 was assigned to them.

Phenotypic Identification of marine *B. subtilis* CBPPR1

To discern the phenotypic characteristics of marine *B. subtilis*, a swift biochemical identification assay using the KB001 test kit from Himedia, India was conducted. To visualise the spores, an endospore staining method was employed, and FE-SEM manufactured by TESCAN, headquartered in the Czech Republic, was employed to scrutinise the morphology of the CBPPR1 bacterial culture.

Genotypic Identification of marine *B. subtilis* CBPPR1

To elucidate and establish the phylogenetic connections of CBPPR1, PCR amplification of the bacterial 16s rRNA gene was performed using primers specified in the protocol outlined by Edwards et al (Dykman and Khlebtsov, 2011). Subsequently, the PCR products were purified and sequenced by the Yaazh Xenomics Research Laboratory in Coimbatore, India. To ascertain its taxonomic affiliation, the CBPPR1 sequence was compared against previously documented sequences using BLAST software. The alignment of the CBPPR1 16s rRNA gene sequence with those from genera sharing phylogenetic proximity was performed using MEGA software. Bacterial gene sequence submitted NCBI gene bank (Accession number: SUB13929013) and the sequence data publicly release 02-01-2025.

Marine *B. subtilis* CBPPR1 cultivation and extraction

B. subtilis bacteria were cultivated for 24 hr in 10 mL test tubes containing Zobell marine culture medium. Following this initial incubation period, the inoculum was transferred into 500 mL of liquid Zobell Marine medium and incubated at room temperature for five days. After five days of incubation, the B. subtilis culture was subjected to centrifugation to harvest the cell-free extract, which was subsequently utilised in the synthesis of gold and silver nanoparticles.

Synthesis of AuNPs and AgNPs through aqueous extraction facilitated by CBPPR1

Microwave-assisted gold nanoparticle synthesis

B. subtilis extract and gold chloride (3mM) were mixed in the ratio of 5:1. The solution was heated in a domestic microwave oven until its brown colour changed. Changes in colour and the time taken for colour change were recorded. Standard procedures were adopted (Chithambharan et al., 2021).

Photo-assisted silver nanoparticle synthesis

The *B. subtilis* extract and $AgNO_3$ were mixed in the ratio of 5:1 and placed under sunlight until a visible colour change of the colloidal solution was observed.

Purification of CBPPR1 AuNPs and AgNPs

The synthesised CBPPR1 AuNPs and AgNPs were purified by centrifuging the solutions thoroughly to remove debris from the bacterial extract and obtain purified nanoparticles. Purified nanoparticles were used for analytical characterization.

Characterization of CBPPR1 AuNPs and AgNPs

Analysis of the structural and morphological characteristics of the bacterial extract-synthesized CBPPR1 Au and AgNPs was carried out using a number of methods, including Bio spec Nano (Shimadzu-Japan), which measures the surface plasmon resonance of nanoparticles. ATR-FTIR spectrometry was used to determine the functional groups of extracts that were responsible for reducing gold chloride and silver nitrate, and forming gold and silver nanoparticles, respectively (Shimadzu IR affinity-Japan). The nanoparticles were covered with an ATR (ZnSe) substrate, and an X-ray diffractometer (XPERT-PRO-UK) was used to study the crystalline nature of the nanoparticles. Field emission scanning electron microscopy (FE-SEM, TESCAN-Czech Republic) and

high-resolution transmission electron microscopy (HRTEM, JEOL Ltd., Japan) were used to identify the microscopic nature and surface morphology of the nanoparticles. A Zetasizer Nano ZS (Malvern Instruments-UK) was used to evaluate the particle size and zeta potential of the liquid suspensions.

Culture media and clinical microorganisms

CBPPR1 AuNPs and AgNPs were examined for antimicrobial activity against clinically significant microorganisms. Clinical *E. coli*, *K. pneumoniae*, and *S. aureus* were obtained from the Clinical Microbiology Lab in Coimbatore, India. Each culture was subcultured separately in 5 mL of sterile nutrient broth and incubated for 24 h at 37°C. The cultures were adjusted to match the turbidity of the MacFarland standards.

CBPPR1 AuNPs and AgNPs antibacterial activity by disc-diffusion method

To investigate the potential antimicrobial properties of both CBPPR1 AuNPs and AgNPs, a well-diffusion method was employed. Fresh agar plates were prepared using double-strength Mueller Hinton agar (MHA) medium (7.6 g in 100 mL) previously sterilised by autoclaving at 121°C for 15 min (Himedia). Clinical microbial cultures were evenly spread onto the surfaces of MHA plates using sterile cotton swabs. Wells were then created in agar using a sterile borer, and 100 µL of either CBPPR1 AuNPs or AgNPs was aseptically added in duplicate. As a control, ciprofloxacin (10 µg/mL) was introduced into the agar wells. To allow diffusion of AuNPs and AgNPs into agar, the culture plates were refrigerated for 30 min. The plates were then incubated at 37°C for 24 hr. The antibacterial activity was assessed using a zone reader (HiMedia).

Determination of minimal inhibitory concentration for CBPPR1 AuNPs and AgNPs

The assay was performed as described by Moussa et al. (Bruna et al., 2021), with some modifications. Different concentrations of AuNPs and AgNPs (500, 250, 125, 62.5, 31.25, 15.625, and 7.8125 µg/mL) and the respective controls were added to 1.0 mL cell culture plates. 100µL of the test microorganism was added to each well. The plates were incubated overnight at room temperature for 24 h, and MIC was measured.

FE-SEM and HR-TEM examine antimicrobial effects of CBPPR1 AuNPs and AgNPs

The bacteria were subjected to treatment with MIC concentrations of 125 µg, 62.5 µg of CBPPR1 AuNPs and AgNPs. After 24 h of incubation, the cells were centrifuged, washed twice, and finally resuspended in phosphate-buffered saline (PBS). Subsequently, the bacterial cells were fixed for 2 h at room temperature using a 2.5% glutaraldehyde solution. Following fixation, they were dehydrated with alcohol, dried using hexamethyldisilazane (HMDS), and finally coated with a layer of gold. FE-SEM and HR-TEM were employed to investigate the impact of CBPPR1 Au and AgNPs on bacterial cells. FE-SEM was conducted using TESCAN equipment. The process for sample preparation for HR-TEM mirrored that of SEM, with the exception that a drop of the bacterial suspension was placed onto a copper grid and allowed to dry. The grids were subsequently examined at 200 kV using a JEM-2100PLUS TEM device (JEOL Ltd., Japan).

Cytotoxicity of CBPPR1 AuNPs and AgNPs

Maintenance of HT-29 and HT-116 cell lines

The National Center for Cell Sciences (NCCS) in Pune, India houses a cell repository from which HT-29 and HT-116 (human colorectal cancer cell lines) were obtained. In a modified Eagle's medium (DMEM) supplemented with 10% foetal bovine serum, these cells were fed and kept alive (FBS). Penicillin and streptomycin (100 g/mL) were added to the growth medium to prevent bacterial contamination. The cell cultures were carefully kept under controlled conditions, precisely at 37°C for 24 hr, in a humidified environment that was enhanced with 5 percent CO_2.

MTT assay of CBPPR1 AuNPs and AgNPs

A modified cell viability experiment was used to determine the cytotoxicity of CBPPR1 AuNPs and AgNPs towards HT-29 and HT-116 cells. The procedure has been described by Mosmann et al (Edwards et al., 1989). The cells were plated in 96-well plates (100 L for each well), counted using a hemocytometer, and diluted in DMEM to a density of 1104 cells/mL. The cells were then allowed to attach for 24 hr at 37°C in a humid environment with 5% CO_2.

Each cell line was subsequently exposed to control medium and different doses of AuNPs and AgNPs, ranging from 0 to 500 g/mL, and cultured for 24 hr at 37°C in a humidified incubator with 95 percent air and 5 percent CO_2. After incubation, the cells that had been exposed to the CBPPR1AuNPs and AgNPs were flushed with new culture medium, MTT (5 mg/mL in PBS) dye was added to each well, and the cells were incubated for an additional 4 hr at 37°C. The cell viability was measured at 540 nm using a microplate reader. The proportion of viable cells in the control wells represents the number of viable cells. Half-maximal inhibitory concentration (IC_{50}) values were calculated and the optimal dosages over time were determined.

$$\text{Proliferation inhibition (\%)} = (\text{Optical density of control} - \text{Optical density of test}) \times 100$$

The IC_{50} values were calculated using the dose-response curve of CBPPR1AuNPs and AgNPs, which showed a 50% decrease in cytotoxicity compared to control cells. Each experiment was performed in duplicate.

Acridine orange/ethidium bromide staining technique was used to measure induction of apoptosis.

Fluorescence microscopic examination of apoptotic cell death was conducted following the protocol described by Liu et al. (2021). To create a dye mixture, 100 µL of equal parts of acridine orange and ethidium bromide were dissolved in PBS. HT-29 and HT-116 cells were seeded in a 96-well plate at a density of 5 × 104 cells per well and allowed to incubate for 24 hr. Subsequently, the cells were detached, washed with cold PBS, and stained with a solution containing acridine orange (100 µg/mL) and ethidium bromide (100 µg/mL) at room temperature for 5 min, following a 24 hr treatment with CBPPR1 AuNPs and AgNPs. Stained cells were examined using a fluorescence microscope at 40x magnification. The percentage of apoptotic cells per field was calculated relative to the total cell count within the field.

Annexin V apoptosis assay

The apoptosis assay was carried out using the ANNEXIN A5-FITC-Apoptosis Detection Kit (Beckman Coulter), following the manufacturer's protocol. Briefly, the cell pellets from the control and AuNPs and AgNP-treated groups were resuspended in 1X binding buffer to 5×10^6 cells/ml. Then, 1µL of annexin A5-FITC and 5µL of PI were added to the samples, which were incubated on ice for 15 min and analysed using flow cytometry.

In-vivo wound healing assay

A study involving 24 male albino rats was conducted to assess the efficacy of CBPPR1AgNPs in promoting wound healing. The rats were divided into four groups, with six animals in each group: a negative control group without drug (G1), a group treated with a concentration of 62.5 µg CBPPR1AgNPs (G2), a group treated with 125 µg CBPPR1AgNPs (G3), and a positive control group treated with commercial silver sulfadiazine ointment (10 mg/g) (G4). Ethical clearance for the experiment was obtained from the Animal Ethics Committee of the Cape Bio Lab and Research Centre, Marthandam, KK District, Tamil Nadu, and the study was approved by the CBLRC/IAEC/10/01-2023.

The experiment began by subjecting the rats to moderate ether anaesthesia to induce a state of sedation. Subsequently, the backside of the mice was shaved using an electric clipper, and the shaved region was thoroughly sterilised using a 70% ethanol solution. Wounds with a diameter of 10 mm were carefully created using scissors. To introduce the infection, all wounds were inoculated with a 50 µL suspension of *S. aureus* bacteria (Arafa et al., 2018; Golmohammadi et al., 2020). Group G1 was the negative control without any treatment, while groups G3 and G4 received CBPPR1AgNPs at varying concentrations. Over 16 days, all three groups were treated twice daily, and the progress of wound contraction was monitored. The wound area of each rat was measured on days 0, 4, 8, 12, and 16 after the wound creation. The percentage wound contraction was calculated using the following formula: Initial wound size-Specific day wound size/ Initial wound size × 100.

Histopathological analysis

At the end of the experimental study (after a 16-day period), animals were euthanised in a CO_2 chamber. Autopsy samples were collected from the rats for histopathological examination. The kidneys and livers were harvested for CBPPR1AgNPs acute toxicity assessment. The samples were immersed in 10% formalin solution for 24 h, rinsed with tap water, and diluted with alcohol. Xylene was used as a clearing agent. Tissue blocks were prepared using a sledge microtome and the sections were de-paraffinised. H&E staining was used to examine cellular and tissue structures under a light microscope.

Statistical analysis

The data is presented as mean values along with their respective standard deviations (SD), and these values were derived from a minimum of three independent experiments. Statistical analysis was conducted using GraphPad software. To compare two groups, a two-sided unpaired Student's t-test was employed. For comparisons involving more than two groups, one-way ANOVA was utilised for statistical evaluation. The significant levels are indicated as follows: *p< 0.05, **p< 0.01, and ***p< 0.001.

Results

Marine *B. subtilis* isolation

One colony was isolated from a crowded plate (marine sediment bacterial colonies) with identical morphology on Zobell marine agar (Figure 1) for further purification and characterisation. Purified marine *B. subtilis* was cultured in Zobell medium. All the bacterial growth analyses were conducted under aseptic conditions.

Phenotypic identification

B. subtilis is a gram-positive bacterium that exhibits high viscus and thick extracellular secretion (Figure 1B), spore formation, and facultative anaerobic growth. The bacterial cell morphology was observed using a scanning electron microscope (Figure 2). The results of biochemical assays performed on the marine *B. subtilis* strain are summarised in Table 1.

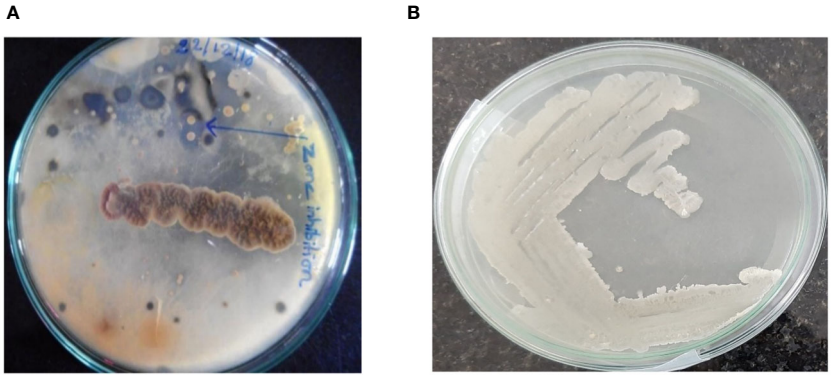

FIGURE 1
(A) Marine bacteria CBPPR1 from crowded plates; **(B)** Purified CBPPR1 marine bacillus.

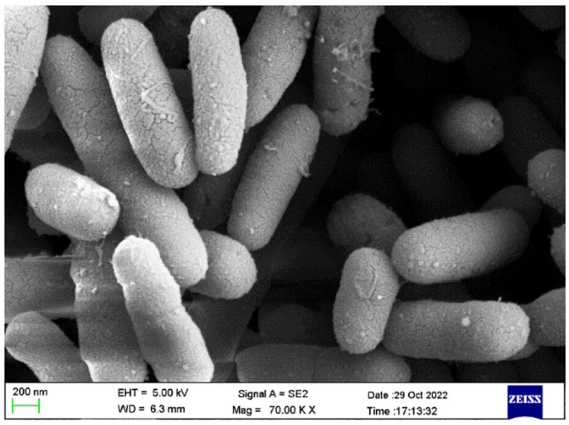

FIGURE 2
Scanning electron microscopy images of marine *B subtilis* (CBPPR1).

Genotypic identification of the marine *B. subtilis*

Phylogenetic analysis of the 16S rRNA gene sequence (1250 bp) revealed that *B. subtilis* occupies a distinct position within the phylum Firmicutes and belongs to the family Bacillaceae, as depicted in Figure 3.

Preparation of gold and silver nanoparticles

The observable alteration in the colour of the colloidal solution served as confirmation of the synthesis of both gold (Au) and silver (Ag) nanoparticles, as depicted in Figure 4. The B. subtilis extract exhibited efficient reduction capabilities for converting Au^{3+} and Ag^{2+} ions, which could be attributed to the presence of active secondary metabolites in the CBPPR1 extract. By subjecting the solution to consistent microwave heating, gold nanoparticles were rapidly formed, substantiated by the noticeable colour transition from brown to pink, as indicated in Tables 2A, B.

Similarly, the formation of Ag2 + to Ag° was confirmed by the rapid visual colour change of the colloidal solution, which occurred within approximately 3 min. These results show that eco-friendly synthesis of metallic nanoparticles such as gold and silver is possible using CBPPR1 extract. The synthesized eco-friendly synthesis of metallic nanoparticles such as CBPPR1AuNPs and AgNPs were purified by using ultra centrifugation.

UV-Visible spectroscopy of CBPPR1 Au and AgNPs

The UV-visible spectra of CBPPR1AuNPs showing SPR at 540 nm, shown in Supplementary Figure S1B, confirm the formation of AuNPs, while Supplementary Figure S1C shows the spectra of CBPPR1Ag with SPR at 445 nm, confirming the formation of AgNPs. The position of the maximum absorption of

TABLE 1 Phenotypic characteristics of CBPPR1.

Test	Results
Citrate	+
Glucose test	+
Adonitol test	+
Arabinose test	+
Lactose test	+
Sorbitol test	+
Mannitol test	+
Rhamnose	+
Sucrose test	+
Starch hydrolysis test	+
Indole test	–
Methyl red	–
Voges Proskauer's	–

(-), Absent; (+), Present.

FIGURE 3
The phylogenetic tree, based on 16S rRNA gene sequences, illustrates the taxonomic relationship between strain CBPPR1 (*B. subtilis*) and various other bacillus species within the genus.

polydisperse colloids does not provide any information about the size of the nanoparticles, as the observation of peak separation in these colloids is not feasible. For the combination of multiple nanoparticles, the plasmon resonance will show a longer wavelength than that of single nanoparticles. Thus, aggregation may be observed as an intensity increase in the near-infrared spectral area (Jin et al., 2020).

FT-IR spectroscopy analysis of CBPPR1 Au and AgNPs

The CBPPR1 extract (Supplementary Figure S2A) and CBPPR1Au exhibited similar spectra with regard to their functional groups. However, in the CBPPR1Au spectrum, a faint C-metal peak appeared at 493 cm^{-1} (Supplementary Figure S2B), providing conclusive evidence for the formation of gold nanoparticles. A comparable peak at 455 cm^{-1} was also evident in CBPPR1Ag (Supplementary Figure S2C), confirming the presence of AgNPs. Common to all these spectra were prominent broad peaks around 3348 cm^{-1}, indicating the presence of hydroxyl (-OH) groups, and around 1635 cm^{-1}, signifying the stretching vibration of the carbonyl group (C=O).

XRD analysis of CBPPR1 Au and AgNPs

The XRD examination verified the nanoparticles' crystalline composition, as indicated by the diffraction peaks at $2\theta = 38.83$ for CBPPR1Au and $2\theta = 32.40$ and 38.78 for CBPPR1Ag (Supplementary Figure S3).

Zeta potential and Zeta size of CBPPR1 Au and AgNPs

The stability and size of both AuNPs and AgNPs were assessed at 25°C using a zeta sizer. The particle sizes were determined to be 83.19 nm for CBPPR1Au (Supplementary Figure S4A) and 265.4 nm for CBPPR1Ag (Supplementary Figure S4B) respectively. AuNPs and AgNPs showed zeta potential values of -23.9 mV and -22.5 mV respectively, which signify the prevalence of negative surface charges on the synthesized AuNPs and AgNPs. This negative charge imparts a crucial electrostatic repulsion between particles, mitigating the tendency for agglomeration or precipitation. The robust negative zeta potential highlights the colloidal stability of AuNPs and AgNPs in the aqueous environment, a critical attribute for applications ranging from drug delivery systems to biomedical imaging.

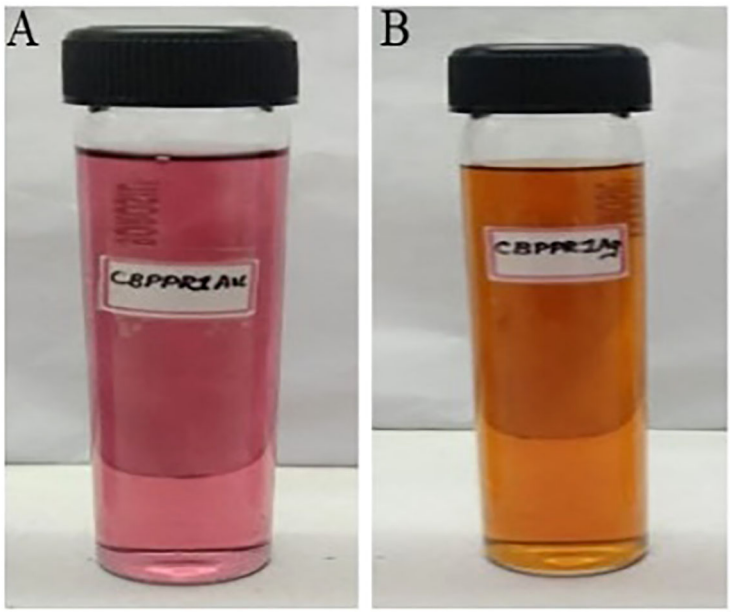

FIGURE 4
CBPPR1Au and AgNPs. **(A)** Gold nanoparticle synthesis and their sample code. **(B)** Silver nanoparticle synthesis and their sample code.

TABLE 2A Gold nanoparticle synthesis and their sample code.

Marine bacillus subtilus aqueous extract (ml)	The volume of $HAuCl_4$ (ml)	Time of formation of gold nanoparticle (s)	Colour of nanoparticle	Sample code
50	10	61	Pink	CBPPR1AuNPs

TABLE 2B Silver nanoparticle synthesis and their sample code.

Marine bacillus subtilus extract (ml)	The volume of $AgNO_3$ (ml)	Time of formation of silver nanoparticle (min)	Colour of nanoparticle	Sample code
50	10	3	Brown	CBPPR1AgNPs

Examination of CBPPR1 Au and AgNPs morphology by FESEM and HRTEM

The FESEM and HRTEM morphological analysis of CBPPR1Au and CBPPR1Ag revealed that the particles exhibited a spherical or oval shape, with sizes ranging from 11.125 nm to 22.484 nm. The morphological features of CBPPR1Au and CBPPR1Ag are presented in Figures 5, 6 respectively.

Energy dispersive X-ray analysis of CBPPR1 AuNPs and AgNPs

EDAX spectroscopy was utilized to determine the elemental composition of the surfaces of the biologically synthesized nanomaterials. In Figures 6D, H, a typical TEM-EDX point-detection example demonstrates the concurrent presence of both gold and silver elements on the surface CBPPR1 AuNPs and AgNPs.

Antimicrobial activity of CBPPR1 AuNPs and AgNPs

To assess the antimicrobial activity of CBPPR1 AuNPs and AgNPs against clinically significant microorganisms, agar-well diffusion method was employed. In this method, plates containing a layer of the relevant clinical microorganism were used. The diameters of the observed zones of inhibition were measured, and the outcomes are presented in Table 3 and Supplementary Figure S5.

Determination of MIC for CBPPR1 Au and AgNPs against clinical microorganisms using serial dilution method

Table 4 serves as a testament to the formidable antibacterial potential of CBPPR1 AuNPs and AgNPs against the clinical microorganism *S. aureus*. At concentrations of 125 µg and 62.5 µg, they exhibited MIC that highlight their potency in restraining the growth of S. aureus. This strategic alliance signifies a precise and effective approach to microbial control, with CBPPR1 AuNPs and AgNPs acting in harmony to create a robust defence against the clinical challenges posed by *S. aureus*. The values presented in Table 4 not only quantify their inhibitory prowess but also open a promising avenue for the development of targeted antibacterial strategies in the ongoing battle against microbial threats.

Scanning electronic microscopy observation

Morphological changes, such as cell shrinking and cell wall lysis were observed in bacterial cells treated with CBPPR1 AuNPs, AgNPs and untreated cells under FE-SEM and HR-TEM (Figures 7, 8).

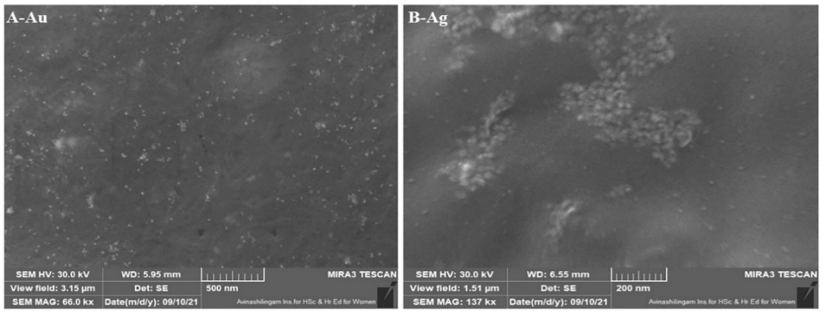

FIGURE 5
(A) Au: CBPPR1AuNPs and **(B)** Ag: CBPPR1AgNPs.

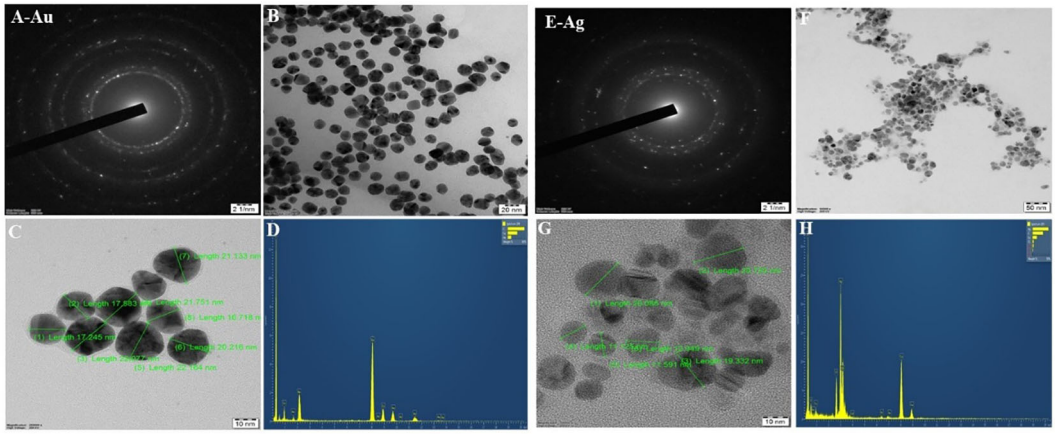

FIGURE 6
HR-TEM and EDAX **(A)** CBPPR1AuNPs with a selected area electron diffraction (SAED) pattern. **(B)** CBPPR1AuNPs at a scale of 200 nm. **(C)** CBPPR1AuNPs on a scale of 10 nm. **(D)** EDAX elemental compositions of CBPPR1AuNPs. **(E)** CBPPR1AgNPs with selected area electron diffraction (SAED) patterns. **(F)** CBPPR1AgNPs at a scale of 50 nm. **(G)** CBPPR1AgNPs at the scale of 10 nm and **(H)** EDAX elemental compositions of CBPPR1AgNPs.

TABLE 3 Antimicrobial activity of CBPPR1 Au and AgNPs and standard drugs against *E. coli, S. aureus* and *K. pneumonia*.

S.NO	Microorganism	Zone of Inhibition (mm) (n=2)		
		CBPPR1 AuNPS (100 µg/mL)	CBPPR1 AgNPs (100 µg/mL)	Ciprofloxacin (10 µg/ml)
1	*E. coli*	13	13	35
2	*S. aureus*	21	22	24
3	*K. pneumoniae*	18	18	18

Figures 7, 8 showed the antibacterial activity of CBPPR1 AuNPs and AgNPs. CBPPR1 AuNPs and AgNPs showed antibacterial activity at concentrations of 125 µg and 62.5 µg (MIC) and emerged as potent inhibitors of *S. aureus* growth. FESEM allows careful observation of the bacterial strain, capturing the aftermath of nanoparticle intervention. Surface observations of the bacterial cells showed the inhibitory ability of AuNPs and AgNPs, a visual indication of their efficacy in restraining the growth of *S. aureus*. High-resolution HRTEM allows for discernment of cell lysis and damage to the bacterial cell wall. The observed cell lysis and damage to the bacterial cell wall are tangible evidences of their formidable antibacterial activity.

3-(4,5-dimethylthiazol-2-yl)-2,5-diphenyltetrazolium bromide assay

MTT assay revealed the cytotoxic activity of CBPPR1 AgNPs and AuNPs. After 24 h of exposure, CBPPR1 AgNPs and AuNPs emerged as dual-edge agents against HT-29 and HT-116 cells. The IC_{50} values of 15.5 µM and 31.25 µM for HT-29 cells attest to the pronounced impact of CBPPR1 AgNPs and AuNPs respectively, signalling a notable sensitivity of these cells to the CBPPR1 AgNPs and AuNPs (Figure 9; Table 5). Similarly, the IC_{50} value of 62.5 µg for HT-116 cells underscores the potency of CBPPR1 AgNPs and AuNPs in impeding cell viability (Figure 9; Table 6). These findings not only reveal the nuanced dynamics of nanoparticle-cell interactions but also pave the way for the exploration of targeted cytotoxic strategies, positioning CBPPR1 AgNPs and AuNPs as promising contenders in the pursuit of selective anticancer interventions.

Fluorescent staining for apoptosis

To explore the potential morphological shifts in HT-29 and HT-116 cell lines upon exposure to CBPPR1AuNPs and AgNPs, acridine orange/ethidium bromide (AO/EB) staining was employed, as illustrated in Supplementary Figure S6. This staining methodology served as a lens for investigating the apoptotic features induced by CBPPR1AuNPs and AgNPs in these cell lines. The fluorescent patterns arising from AO/EB staining provided a dynamic representation of cell viability and membrane integrity. Cells transitioning towards demise became permeable to ethidium bromide (EB), emitting an orange-red fluorescence, whereas viable cells exhibited permeability to acridine orange (AO), emanating a vibrant green fluorescence. Therapeutic interventions instigated four distinct cytological and morphological changes in AO/EB-stained nuclei: thriving cells displaying well-organised nuclei, early apoptotic cells characterised by nuclear condensation, and late apoptotic cells exhibiting condensed or fragmented chromatin. This nuanced exploration through fluorescence staining sheds light on the intricate interplay between CBPPR1AuNPs and AgNPs and the

10.3389/fmars.2024.1284813

TABLE 4 MIC of CBPPR1 Au and AgNPs against the clinical microorganism *S. aureus*.

S.NO	Microorganism	MIC (n=2)	
		CBPPR1AuNPs	CBPPR1AgNPs
1	*S. aureus*	125 µg	62.5 µg

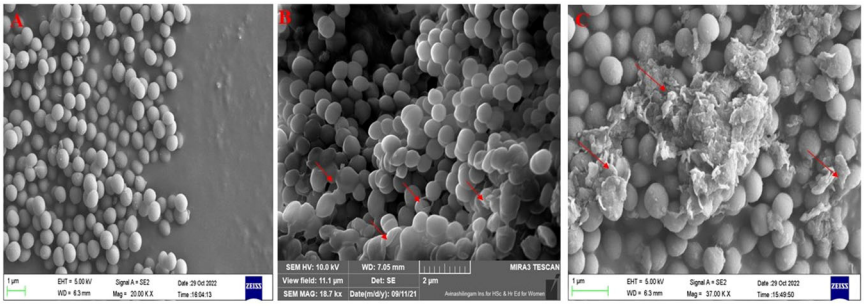

FIGURE 7
FE-SEM images: **(A)** untreated *S. aureus*, **(B)** CBPPR1AuNPs treated *S. aureus*. **(C)** CBPPR1AgNPs treated *S. aureus*.

cellular landscape, revealing the apoptotic signatures in HT-29 and HT-116 cells.

Apoptosis measured by flow cytometry

Figure 10 presents a glimpse into cellular dynamics through fluorescence-activated cell sorting (FACS), offering detailed insight into the impact of CBPPR1Au and AgNPs on cell fate. In Figures 10A–F, the statistical analysis reveals a nuanced story of cellular responses, particularly in terms of early and late apoptosis. Notably, the cell histogram shows a reassuring picture at low concentrations, indicating that CBPPR1Au and AgNPs did not elicit cytotoxic effects. However, as the concentration was increased, a transformation occurred. At higher doses of CBPPR1Au and AgNPs, a substantial shift toward toxicity was apparent in HT-29 and HT-116 cells. This was manifested in early and late apoptosis rates of 42.36% and 38.93%, respectively, in stark contrast to the control group. These findings underscore the concentration-dependent nature of CBPPR1Au and the impact of AgNPs, revealing their potential as agents that induce programmed cell death in cancer cell lines. This FACS-based statistical analysis provides a quantitative dimension for understanding nanoparticle-induced cytotoxicity, which is crucial to discern the intricacies of their influence on cellular fate.

In-vivo wound healing assay

A comprehensive cutaneous wound model involving *S. aureus* infection was established to assess the effectiveness of CBPPR1AgNPs in facilitating wound healing. For *in-vivo* experiments, rats were categorized into four groups: untreated (G1, negative control), treated with CBPPR1AgNPs at a concentration of 62.5 µg/ml (G2), treated with CBPPR1AgNPs at a concentration of 125 µg/ml (G3), and treated with 10 mg/g silver sulfadiazine (G4). As shown in Figure 11, the progression of wound healing was documented using digital camera images. In the control group, wound sites exhibited yellowish pus on days 2 and 4, accompanied by a reddish appearance, indicating ongoing inflammation. In contrast, minimal pus formation was observed in G2, G3, and G4 throughout the treatment period, differentiating them from the control and CBPPR1AgNPs-treated groups. Furthermore, wounds treated with CBPPR1AgNPs (62.5 and 125 µg/ml), and silver sulfadiazine (10 mg/g) exhibited accelerated closure by day 4, signifying effective control of *S. aureus*-induced infections.

By day 16, wound contraction in rats treated with CBPPR1AgNPs (62.5 and 125 µg/ml) and silver sulfadiazine (10 mg/g) had markedly increased, with measurements ranging from initial values of 6.52 ± 1.60 to 96.20 ± 1.78*, 10.55 ± 2.60 to 98.92 ± 1.60**, and 12.30 ± 5.40 to 99.28 ± 0.08**, respectively (Table 7, Figure 11). Notably, wounds treated with CBPPR1AgNPs at a concentration of 125 µg/ml displayed complete closure, with new epidermal tissue covering the area. However, the wounds in G1 remained unhealed (Figure 12).

These findings indicate that CBPPR1AgNPs play a pivotal role in promoting wound healing, mainly because of their potent antibacterial properties. Importantly, the quicker healing rate observed in CBPPR1AgNPs-treated wounds compared to those in the control group could be attributed to the dual benefits of CBPPR1AgNPs, augmenting wound healing and providing a physical barrier that impedes bacterial intrusion into adjacent tissues.

Histopathology

The histopathological assessment of the metabolic organ of the experimental rat kidney tissue samples revealed a lack of anomalies in both the cortex and medulla regions. The glomerular structures

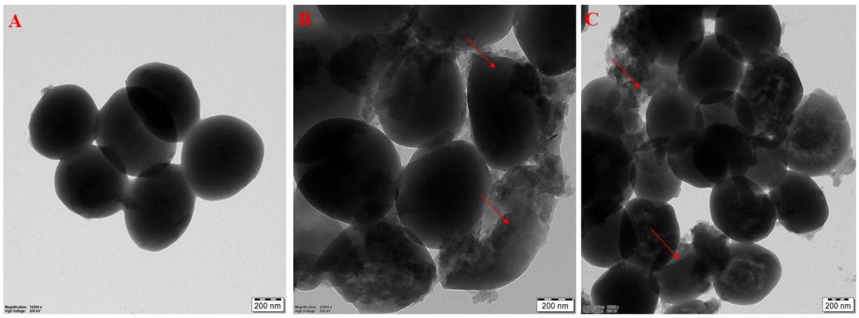

FIGURE 8
HR-TEM images: **(A)** untreated *S. aureus*, **(B)** CBPPR1AuNPs treated *S. aureus*. **(C)** CBPPR1AgNPs treated *S. aureus*.

exhibited a typical and unaltered morphology, reflecting their normal function. Equally, the configuration of the tubulointerstitial compartments demonstrated the anticipated appearance, indicating an absence of any noteworthy changes (Supplementary Figure S8). Furthermore, the blood vessels within the examined tissue displayed an unremarkable appearance, signifying their regular state. Importantly, the absence of signs related to tubular necrosis or inflammation was a notable finding in the kidney samples, suggesting that these pathological processes were not evident. Moving to the liver tissue, the lobular architecture, a fundamental structural aspect was observed to adhere to its characteristic pattern. On the level of individual hepatocytes, no overt indications of pathology were discernible upon microscopic examination, emphasizing their overall healthy appearance (Supplementary Figure S9).

The microscopic examination of kidney sections (Supplementary Figure S8) in Group 1 (negative control) exhibited typical glomerular morphology, healthy tubules, and an absence of apparent interstitial disease, with visible blood vessel congestion. Similarly, Group 2 (CBPPR1AgNPs-62.5 µg/ml), Group 3 (CBPPR1AgNPs-125 µg/ml), and Group 4 (Silver sulfadiazine) demonstrated kidney segments with no obvious pathology in the cortex and medulla, including tubules, interstitium, and blood vessels. In Group 2, only a few clogged blood vessels were noted, while in Groups 3 and 4, there were minimally dilated blood vessels and minor blood vessel congestion, respectively. These observations suggest that CBPPR1AgNPs at concentrations of 62.5 µg/ml and 125 µg/ml, as well as silver sulfadiazine, did not induce significant kidney pathology, maintaining a kidney structure comparable to the negative control group.

Microscopic examination of liver (Supplementary Figure S9) from Group 1 (negative control) revealed a typical lobular architecture with no apparent pathology in hepatocytes, portal triad, central vein congestion, and dilation. Furthermore, there was no discernible pathology in sinusoids. Similar observations were made for Group 2 (CBPPR1AgNPs-62.5 µg/ml), Group 3 (CBPPR1AgNPs-125 µg/ml), and Group 4 (Silver sulfadiazine). In all cases, the liver slices exhibited typical lobular architecture, and no pathology was observed in hepatocytes, portal triad, central vein congestion, dilation, or sinusoids under the microscope. These findings suggest that CBPPR1AgNPs at both 62.5 µg/ml and 125 µg/ml concentrations, as well as silver sulfadiazine, did not induce any observable liver pathology, mirroring the characteristics of the negative control group.

Discussion

Visible colour change is an important observable parameter that indicates the formation of metallic nanoparticles, such as gold and silver nanoparticles. Noble metal nanoparticles possess this unique property of vibrant colour in the visible region because the electrons on the surface of the nanoparticles oscillate, a phenomenon called

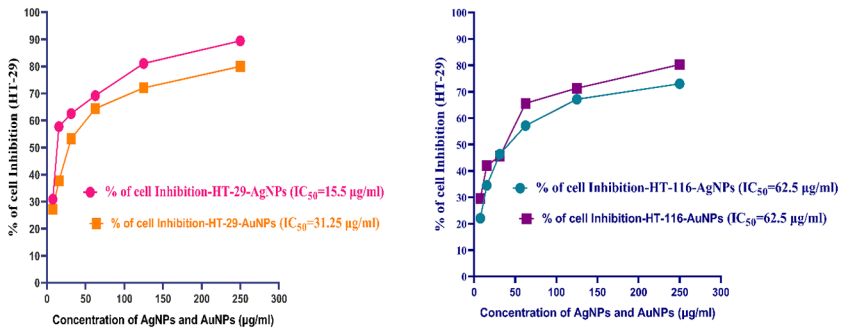

FIGURE 9
Cytotoxicity of CBPPR1AuNPs and AgNPs in HT-29 and HT-116 cell lines.

10.3389/fmars.2024.1284813

TABLE 5 Cytotoxicity of CBPPR1AgNPs and AuNPs in HT-29 cell lines.

Conc., of AgNPs and AuNPs (µg/ml)	% of cell Inhibition-HT-29-AgNPs	% of cell Inhibition-HT-29-AuNPs
250	89.472	80.00
125	81.122	72.077
62.5	69.200	64.466
31.25	62.596	53.249
15.5	57.737	37.687
7.5	30.927	27.22

TABLE 6 Cytotoxicity of CBPPR1AgNPs and AuNPs in HT-116 cell lines.

Conc., of AgNPs and AuNPs (µg/ml)	% of cell Inhibition-HT-29-AgNPs	% of cell Inhibition-HT-29-AuNPs
250	73.039	80.314
125	67.187	71.393
62.5	57.169	65.619
31.25	46.363	45.597
15.5	34.532	42.025
7.5	22.069	29.539

plasmon resonance (Kathiravan et al., 2014). Surface plasmon resonance (SPR) is one of the key features of metallic nanoparticles and can be evaluated using UV-visible spectroscopy. From the FT-IR spectra, the formation of gold and silver nanoparticles was confirmed by the presence of a sharp peak in the 450 cm^{-1} region (Figures 4, 5). These peaks corresponded to the C-metal peak (Elbehiry et al., 2019). This particular upward peak was not observed in the FT-IR spectra of the CBPPR1 extract alone, which shows that the CBPPR1 extract acts as a good reducing agent to effectively reduce Au and Ag ions. In addition, the well-dispersed colloidal solution of CBPPR1-aided silver and gold nanoparticles further confirmed that CBPPR1 was a good stabilizing and reducing agent. The crystalline nature of the synthesized nanoparticles can be studied from the XRD analysis, where it is evident from the peaks of CBPPR1Au and AgNPs that the synthesized particles are crystalline. The FE-SEM and HR-TEM images of CBPPR1Au show scattered spherical nanoparticles, and CBPPR1Ag shows packed spherical particles. From the morphographs, it can be observed that the synthesized nanoparticles could withstand a 30 kV applied electrical potential. This, in turn, demonstrates the stability of the synthesized metallic nanoparticles, which suggests that the nanoparticles were formed by completely reducing the CBPPR1 extract. The shape of the nanoparticles and their bioactivity were strongly correlated in this study, which correlates well with reports that spherical-shaped nanoparticles exhibit strong pharma-related activity (Bruna et al., 2021; Mosdam, 1983).

The presence of several antimicrobial compounds (Lipopeptides): lipopeptides, Mycosubtilin, Bacilysin, Basiliskamide A, and Rhizocticin. Antibiotics such as Kanosamine, Pumilin, Zwittermicin A, Amicoumacin A, Dificidin, Bacillaene, and Aurantinins A were found. Chemical compounds, namely Neotrehalosadiamine, Macrolactin A, and Dihydrobacillaene (Kotakonda et al., 2023) are primarily responsible for particle stability, reduction, and distribution. These bioactive compounds interact with Au and Ag in a variety of ways, including amino groups, cysteine residues, and attraction, due to the negative charges of carboxylic groups presented in *B. subtilis* extract.

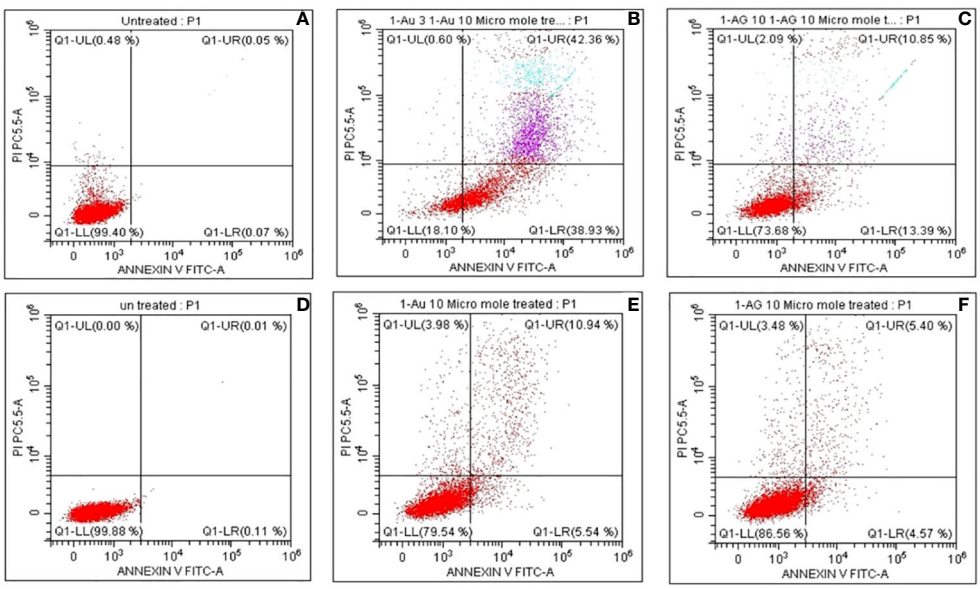

FIGURE 10
The fluorescence scatter images after CBPPR1Au and CBPPR1Ag (10 µg/mL) treatment of HT-29 and HT-116 cells. **(A)** Untreated HT-29 cells. **(B)** CBPPR1Au 10 µg/mL treated HT-29 cells for 24h. **(C)** CBPPR1Ag 10 µg/mL treated HT-29 cells for 24h. **(D)** Untreated HT-116 cells after 24h. **(E)** CBPPR1Au 10 µg/mL treated HT-116 cells for 24h. **(F)** CBPPR1Ag 10 µg/mL treated HT-116 cells for 24h.

10.3389/fmars.2024.1284813

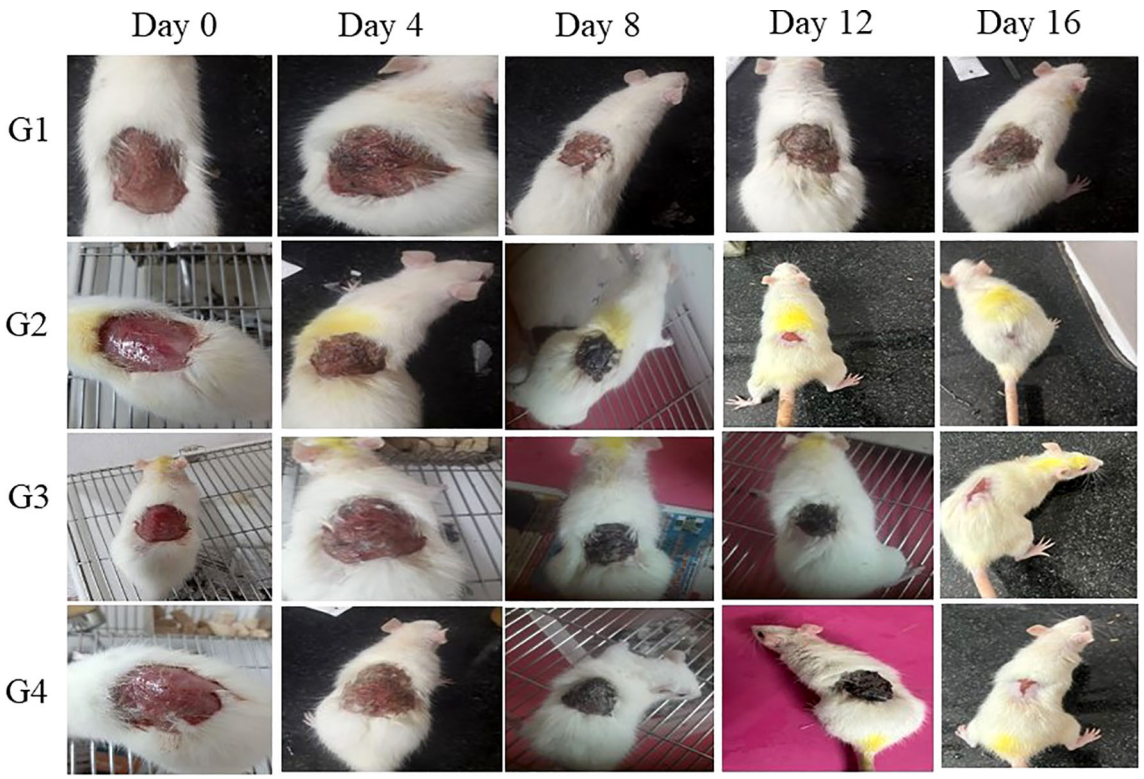

FIGURE 11
In-vivo infected wound healing studies: Representative wound size contraction in four different groups (G1, G2, G3, and G4) on days 0, 4, 8, 12, and 16.

TABLE 7 Effect of CBPPR1AgNPs on wound contraction.

Post wounding days	Dose	Day 0	Day 4	Day 8	Day 12	Day 16
Negative control (G1)	–	4.22 ± 0.81	22.70 ± 09.71	46.70 ± 7.40	74.56 ± 5.10	78.20 ± 2.10
CBPPR1AgNPs (G2)	62.5 µg/ml	6.52 ± 1.60	14.45 ± 1.84	44.71 ± 7.16	87.11 ± 4.80*	96.20 ± 1.78*
CBPPR1AgNPs (G3)	125 µg/ml	10.55 ± 2.60	16.20 ± 08.86	52.26 ± 11.70	82.70 ± 2.75*	98.92 ± 1.60**
Silver sulfadiazine (G4)	10 mg/g	12.30 ± 5.40	22.90 ± 6.10	46.20 ± 4.14*	76.72 ± 3.10**	99.28 ± 0.08**

*Significance.
**Very significance.

The MIC of CBPPR1Ag against a clinical *S. aureus* was measured, and the morphological effects of CBPPR1Ag on the treated bacteria were visualized using SEM and TEM, which revealed the damage and shrinkage of the treated microorganisms (Figures 7, 8). The antibacterial activity of the AgNPs was determined by the size and condition of the nanoparticles. The antibacterial activities of these bio-produced AgNPs against *S. aureus* were significantly effective (Supplementary Figure S7).

The antitumor activities of CBPPR1AuNPs and AgNPs complexes were examined using the HT-29 and HT-116 cell lines. IC_{50} values of CBPPR1AuNPs and AgNPs against HT-29 cell lines respectively 15.5µM and 62.5µg. IC_{50} value of 62.5 µg for HT-116 cells underscores the potency of CBPPR1 AgNPs and AuNPs in impeding cell viability. Ullah reported anticancer activity of biogenic synthesized silver nanoparticles against breast cancer cells (Ullah et al., 2020). Algotiml et al. (2022) demonstrated that the IC_{50} values for the synthesised silver nanoparticles (AgNPs) form marine species were 13 µg/mL and 43 µg/mL, respectively. The AgNPs derived from Ulva rigida exhibited a noteworthy anticancer effect, displaying a substantial 92.62% activity against the MCF-7 human breast adenocarcinoma cell line. In addition, the selectivity of these AgNPs was remarkable; their selectivity index (SI) of 3.2 and IC_{50} value of 13 µg/mL indicated that they exhibited a preferential effect on cancer cells in comparison to normal cells (Algotiml et al., 2022).

The statistical analysis of early and late apoptotic cells was performed by FACS, as shown in Figures 10A-F. The FACS analysis revealed no cytotoxic effects of CBPPR1AuNPs and AgNPs at lower concentrations; however, at higher concentrations they showed high toxicity toward HT-29 and HT-116 cells, leading to early and late apoptosis rates of 42.36% and 38.93%, respectively, compared to the control group.

A cutaneous wound model involving *S. aureus* infection was used to assess the effectiveness of CBPPR1AgNPs in facilitating

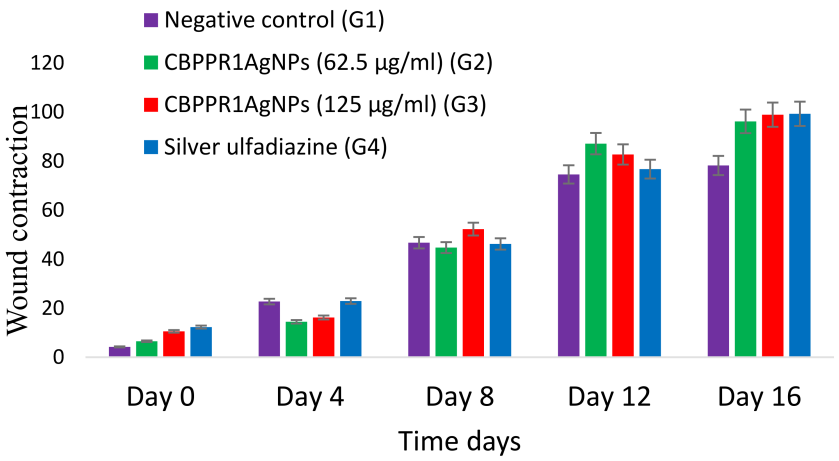

FIGURE 12
Depicting the progressive contraction of wound size across four distinct groups (G1, G2, G3, and G4) on days 0, 4, 8, 12, and 16.

wound healing. *In-vivo* experiments were conducted on rats, categorized into four groups: untreated (G1, negative control), treated with CBPPR1AgNPs (62.5 µg/ml), treated with 125 µg/ml, and treated with silver sulfadiazine (10 mg/g). In the control group, the wound sites exhibited yellowish pus on day four, indicating ongoing inflammation. In contrast, minimal pus formation was observed in groups G2, G3, and G4, indicating the effective control of *S. aureus*-induced infections. The effective antimicrobial activity of CBPPR1AgNPs can be attributed to the presence of bioactive compounds associated with silver nanoparticles (AgNPs).

Wound contraction in rats treated with CBPPR1AgNPs and silver sulfadiazine increased by day 15, with measurements changing from initial values to final values. CBPPR1AgNPs-treated wounds displayed complete closure with new epidermal tissue covering the area. However, wounds in G1 remained unhealed. These findings suggest that CBPPR1AgNPs play a pivotal role in promoting wound healing because of their potent antibacterial properties. The faster healing rate observed in CBPPR1AgNPs-treated wounds compared to those in the control group could be attributed to the dual benefits of augmenting wound healing and providing a physical barrier that impedes bacterial intrusion into adjacent tissues. The histopathological assessment of kidney samples of rat showed no anomalies in cortex and medulla regions; glomerular structures with normal function; tubulointerstitial compartments with no significant changes; and blood vessels with regular appearance. No signs of tubular necrosis or inflammation were found in kidney samples. Hepatocytes showed no overt signs of pathology, emphasizing their overall healthy appearance.

Conclusion

This research highlights a novel approach in the synthesis of CBPPR1Au and AgNPs, leveraging extracts from marine *Bacillus subtilis*. The process not only stands out for its simplicity but also excels in terms of cost-effectiveness and ecological friendliness. The resulting nanoparticles exhibit remarkable antibacterial efficacy against *Staphylococcus aureus*, with CBPPR1AuNPs and CBPPR1AgNPs demonstrating notable inhibitory concentrations (MIC) of 125 µg and 62.5 µg, respectively. Moreover, these nanoparticles showcase substantial cytotoxicity (IC_{50}) against HT-29 (15.5 M) and HT-116 (62.5 M) cell lines, suggesting their potential in combating cancerous cells. In the context of wound healing, the study utilized a cutaneous wound model involving S. aureus infection to assess the effectiveness of CBPPR1AgNPs. *In vivo* experiments conducted on rats revealed minimal pus formation in groups G2, G3, and G4, indicative of the effective control of infections by CBPPR1AgNPs. Notably, wounds treated with CBPPR1AgNPs exhibited complete closure, underscoring their efficacy in the wound healing process. In contrast, wounds in the untreated G1 group remained unhealed. To further evaluate the safety profile of CBPPR1AgNPs, histopathological analysis was conducted on the kidneys and livers of rats. The results indicated no adverse effects, reinforcing the biocompatibility of CBPPR1AgNPs *In vivo*. The collective findings suggest that CBPPR1AgNPs play a pivotal role in wound healing, attributed to their potent antibacterial properties. These nanoparticles emerge as promising candidates for various biological applications due to their environmentally friendly nature. CBPPR1Au and CBPPR1Ag, synthesized through this innovative approach, hold potential for advancing biomedical and therapeutic applications, paving the way for sustainable and effective solutions in the field. Furthermore toxicity, MOA and human trails study needed for human applications.

Data availability statement

The bacterial sequence data presented in the study are deposited in the NCBI Nucleotide repository, accession number OR731140. https://www.ncbi.nlm.nih.gov/nuccore/OR731140.1.

Ethics statement

The animal study was approved by Cape Bio Lab and Research Centred, Laboratory animal facility (CPCSEA reg.No: 2045/po/

RcBiBt/S/18/CPCSEA). The study was conducted in accordance with the local legislation and institutional requirements.

Author contributions

RP: Data curation, Methodology, Conceptualization, Formal analysis, Investigation, Validation, Visualization, Writing – original draft. NA: Data curation, Funding acquisition, Writing – review & editing. HA: Data curation, Funding acquisition, Writing – review & editing. SK: Data curation, Funding acquisition, Writing – review & editing. MA: Data curation, Funding acquisition, Conceptualization, Formal analysis, Investigation, Writing – review & editing. PS: Data curation, Formal analysis, Resources, Conceptualization, Investigation, Writing – review & editing. IU: Data curation, Formal analysis, Resources, Writing – review & editing. LP: Formal analysis, Methodology, Resources, Writing – original draft. AC: Formal analysis, Methodology, Resources, Writing – review & editing. DY: Data curation, Formal analysis, Investigation, Writing – review & editing. ST: Formal analysis, Methodology, Resources, Writing – review & editing. SV: Conceptualization, Data curation, Formal analysis, Investigation, Methodology, Visualization, Writing – review & editing, Resources, Validation, Writing – original draft. SK: Formal analysis, Investigation, Methodology, Resources, Data curation, Validation, Writing – review & editing. MK: Conceptualization, Data curation, Formal analysis, Funding acquisition, Investigation, Methodology, Project administration, Resources, Software, Supervision, Validation, Visualization, Writing – original draft, Writing – review & editing.

Funding

The author(s) declare financial support was received for the research, authorship, and/or publication of this article. This research work was funded by institutional Fund Projects under grant No. (IFPIP: 1768-249-1443). The authors gratefully acknowledge the technical and financial support provided by the Ministry of Education and King Abdulziz University, DSR, Jeddah, Saudi Arabia.

Acknowledgments

I would like to thank the Center for Biotechnology and Phytopharmacognosy Research, Coimbatore, Tamil Nadu, India. This manuscript has been edited by the ICGEB editing service (manuscripts@icgeb.org).

Conflict of interest

The authors declare that the research was conducted in the absence of any commercial or financial relationships that could be construed as a potential conflict of interest.

Publisher's note

Supplementary material

The Supplementary Material for this article can be found online at: https://www.frontiersin.org/articles/10.3389/fmars.2024.1284813/full#supplementary-material

References

Algotiml, R., Gab-Alla, A., Seoudi, R., Abulreesh, H. H., El-Readi, M. Z., and Elbanna, K. (2022). Anticancer and antimicrobial activity of biosynthesized Red Sea marine algal silver nanoparticles. *Sci. Rep.* 12, 2421. doi: 10.1038/s41598-022-06412-3

Arafa, M. G., El-Kased, R. F., and Elmazar, M. M. (2018). Thermoresponsive gels containing gold nanoparticles as smart antibacterial and wound healing agents. *Sci. Rep.* 8, 13674. doi: 10.1038/s41598-018-31895-4

Bharadwaj, K. K., Rabha, B., Pati, S., Sarkar, T., Choudhury, B. K., Barman, A., et al. (2021). Green synthesis of gold nanoparticles using plant extracts as beneficial prospect for cancer theranostics. *Molecules (Basel, Switzerland)* 26 (21), 6389. doi: 10.3390/molecules26216389

Bruna, T., Maldonado-Bravo, F., Jara, P., and Caro, N. (2021). Silver nanoparticles and their antibacterial applications. *Int. J. Mol. Sci.* 22, 7202. doi: 10.3390/ijms22137202

Chithambharan, A., Pottail, L., Mirle, R. M., Rajalakshmi, R., and Ponnusamy, A. (2021). Bioinspired gold nanoparticle synthesis using *terminalia bellerica* fruit parts and exploring their anti-bacterial potency *in vitro*. *Indian J. Microbiol.* 61, 298–305. doi: 10.1007/s12088-021-00937-3

Dubas, S. T., and Pimpan, V. (2008). Green synthesis of silver nanoparticles for ammonia sensing. *Talanta* 76, 29–33. doi: 10.1016/j.talanta.2008.01.062

Dykman, L. A., and Khlebtsov, N. G. (2011). Gold nanoparticles in biology and medicine: recent advances and prospects. *Acta Naturae.* 3, 34–55. doi: 10.32607/20758251-2011-3-2-34-55

Edwards, U., Rogall, T., Blöcker, H., Emde, M., and Böttger, E. C. (1989). Isolation and direct complete nucleotide determination of entire genes. Characterization of a gene coding for 16S ribosomal RNA. *Nucleic Acids Res.* 17, 7843–7853. doi: 10.1093/nar/17.19.7843

Elbehiry, A., Al-Dubaib, M., Marzouk, E., and Moussa, I. (2019). Antibacterial effects and resistance induction of silver and gold nanoparticles against Staphylococcus aureus-induced mastitis and the potential toxicity in rats. *Microbiologyopen* 8, e00698. doi: 10.1002/mbo3.698

Fang, H., Zhang, X., Zhang, S. J., Liu, L., Zhao, Y. M., and Xu, H. J. (2015). Ultrasensitive and quantitative detection of paraquat on fruits skins *via* surface-enhanced Raman spectroscopy. *Sensors Actuators B: Chemical.* 5, 213, 452–6. doi: 10.1016/j.snb.2015.02.121

Fariq, A., Khan, T., and Yasmin, A. (2017). Microbial synthesis of nanoparticles and their potential applications in biomedicine. *J. Appl. Biomed.* 15, 241–248. doi: 10.1016/j.jab.2017.03.004

Fatimah, I. (2016). Green synthesis of silver nanoparticles using extract of *Parkia speciosa Hassk* pods assisted by microwave irradiation. *J. Adv. Res.* 7, 961–969. doi: 10.1016/j.jare.2016.10.002

Ghosh, S., Ahmad, R., Zeyaullah, M., and Khare, S. K. (2021). Microbial nano-factories: synthesis and biomedical applications. *Front. Chem.* 9, 194. doi: 10.3389/fchem.2021.626834

Golmohammadi, R., Najar-Peerayeh, S., Tohidi Moghadam, T., and Hosseini, S. M. J. (2020). Synergistic Antibacterial Activity and Wound Healing Properties of Selenium-

Chitosan-Mupirocin Nanohybrid System: An *in-vivo* Study on Rat Diabetic Staphylococcus aureus Wound Infection Model. *Sci. Rep.* 10, 2854. doi: 10.1038/s41598-020-59510-5

Hu, X., Zhang, Y., Ding, T., Liu, J., and Zhao, H. (2020). Multifunctional gold nanoparticles: A novel nanomaterial for various medical applications and biological activities. *Front. Bioeng Biotechnol.* 8, 990. doi: 10.3389/fbioe.2020.00990

Jin, C., Wang, K., Oppong-Gyebi, A., and Hu, J. (2020). Application of nanotechnology in cancer diagnosis and therapy - A mini-review. *Int. J. Med. Sci.* 17, 2964–2973. doi: 10.7150/ijms.49801

Kambale, E. K., Nkanga, C. I., Mutonkole, B. I., Bapolisi, A. M., Tassa, D. O., Liesse, J. I., et al. (2020). Green synthesis of antimicrobial silver nanoparticles using aqueous leaf extracts from three Congolese plant species (*Brillantaisia patula*, *Crossopteryx febrifuga* and *Senna siamea*). *Heliyon* 6, e04493. doi: 10.1016/j.heliyon.2020.e04493

Kathiravan, V., Ravi, S., and Ashokkumar, S. (2014). Synthesis of silver nanoparticles from Melia dubia leaf extract and their in *vitro* anticancer activity. *Spectrochimica Acta Part A: Mol. Biomol. Spectroscopy.* 15, 130,116–21. doi: 10.1016/j.saa.2014.03.107

Khan, T., Ullah, N., Khan, M. A., Mashwani, Z. U., and Nadhman, A. (2019). Plant-based gold nanoparticles; a comprehensive review of the decade-long research on synthesis, mechanistic aspects and diverse applications. *Adv. Colloid Interface Sci.* 272, 102017. doi: 10.1016/j.cis.2019.102017

Kotakonda, M., Marappan, M., Dharmar, P., Sakthivel, B., and Sunnapu, P. (2023). Isolation and identification of bioactive compounds with antimicrobial activity from marine facultative anaerobe. *Bacillus subtilis. Curr. Pharm. Biotechnol.* 24, 698–707. doi: 10.2174/1389201023666220801090810

Lee, S. H., and Jun, B. H. (2019). Silver nanoparticles: synthesis and application for nanomedicine. *Int. J. Mol. Sci.* 20, 865. doi: 10.3390/ijms20040865

Liu, X., Chen, J. L., Yang, W. Y., Qian, Y. C., Pan, J. Y., Zhu, C. N., et al. (2021). Biosynthesis of silver nanoparticles with antimicrobial and anticancer properties using two novel yeasts. *Sci. Rep.* 11 (1), 15795. doi: 10.1038/s41598-021-95262-6

Loiseau, A., Asila, V., Boitel-Aullen, G., Lam, M., Salmain, M., and Boujday, S. (2019). Silver-based plasmonic nanoparticles for and their use in biosensing. *Biosensors* 9 (2), 78. doi: 10.3390/bios9020078

Mihai, M. M., Dima, M. B., Dima, B., and Holban, A. M. (2019). Nanomaterials for wound healing and infection control. *Mater. (Basel).* 12, 2176. doi: 10.3390/ma12132176

Mosdam, T. J. (1983). Rapid colorimetric assay for cellular growth and survival: application to proliferation and cytotoxic assay. *J. Immunol. Methods* 65, 55–63. doi: 10.1016/0022-1759(83)90303-4

Ramachandran, R., Krishnaraj, C., Sivakumar, A. S., Prasannakumar, P., Abhay Kumar, V. K., Shim, K. S., et al. (2017). Anticancer activity of biologically synthesized silver and gold nanoparticles on mouse myoblast cancer cells and their toxicity against embryonic zebrafish. *Mater Sci. Eng. C Mater Biol. Appl.* 73, 674–683. doi: 10.1016/j.msec.2016.12.110

Singh, A. K., Tiwari, R., Kumar, V., Singh, P., Riyazat Khadim, S. K., Tiwari, A., et al. (2017). Photo-induced biosynthesis of silver nanoparticles from aqueous extract of Dunaliella salina and their anticancer potential. *J. Photochem. Photobiol. B.* 166, 202–211. doi: 10.1016/j.jphotobiol.2016.11.020

Soliman, M. K. Y., Salem, S. S., Abu-Elghait, M., and Azab, M. S. (2023). Biosynthesis of silver and gold nanoparticles and their efficacy towards antibacterial, antibiofilm, cytotoxicity, and antioxidant activities. *Appl. Biochem. Biotechnol.* 195, 1158–1183. doi: 10.1007/s12010-022-04199-7

Ullah, I., Khalil, A. T., Ali, M., Iqbal, J., Ali, W., Alarifi, S., et al. (2020). Green-synthesized silver nanoparticles induced apoptotic cell death in MCF-7 breast cancer cells by generating reactive oxygen species and activating caspase 3 and 9 enzyme activities. *Oxid. Med. Cell Longev.* 2020, 1215395. doi: 10.1155/2020/1215395

Vines, J. B., Yoon, J. H., Ryu, N. E., Lim, D. J., and Park, H. (2019). Gold nanoparticles for photothermal cancer therapy. *Front. Chem.* 7, 167. doi: 10.3389/fchem.2019.00167

Wei, D., Sun, W., Qian, W., Ye, Y., and Ma, X. (2009). The synthesis of chitosan-based silver nanoparticles and their antibacterial activity. *Carbohydr. Res.* 344, 2375–2382. doi: 10.1016/j.carres.2009.09.001

Zhang, X. F., Liu, Z.-G., Shen, W., and Gurunathan, S. (2016). SilverNanoparticles: synthesis, characterization, properties, applications, and therapeutic approaches. *Int. J. Mol. Sci.* 17, 1534. doi: 10.3390/ijms17091534